Pergamon

Available online at www.sciencedirect.com
SCIENCE DIRECT®

Cement and Concrete Research 33 (2003) 1293–1309

CEMENT AND CONCRETE RESEARCH

A multiscale micromechanics-hydration model for the early-age elastic properties of cement-based materials

Olivier Bernard, Franz-Josef Ulm*, Eric Lemarchand

Massachusetts Institute of Technology, Cambridge, MA 02139, USA

Received 1 May 2002; accepted 13 January 2003

Abstract

The *E*-modulus of early age cement-based materials, and more importantly, its evolution in time, is one of the most critical material-to-structural design parameters affecting the likelihood of early-age concrete cracking. This paper addresses the problem by means of a multistep micromechanics approach that starts at the nanolevel of the C–S–H matrix, where two types of C–S–H develop in the course of hydration. For the purpose of homogenization, the volume fractions of the different phases are required, which are determined by means of an advanced kinetics model of the four main hydration reactions of ordinary portland cement (OPC). The proposed model predicts with high accuracy the aging elasticity of cement-based materials, with a minimum intrinsic material properties (same for all cement-based materials), and 11 mix-design specific model parameters that can be easily obtained from the cement and concrete suppliers. By way of application, it is shown that the model provides a quantitative means to determine (1) the solid percolation threshold from micromechanics theory, (2) the effect of inclusions on the elastic stiffening curve, and (3) the development of the Poisson's ratio at early ages. The model also suggests the existence of a critical water-to-cement ratio below which the solid phase percolates at the onset of hydration. The development of Poisson's ratio at early ages is found to be characterized by a water-dominated material response as long as the water phase is continuous, and then by a solid-dominated material response beyond the solid percolation threshold. These model-based results are consistent with experimental values for cement paste, mortar, and concrete found in the open literature.

Keywords: Concrete; Hydration; Elastic moduli; Micromechanics; Percolation threshold

1. Introduction

The elastic or Young's modulus (*E*-modulus) of concrete is important in all structures that are subjected to boundary conditions of displacements that are more or less restrained. Its importance is further amplified when the deformation is restrained from a very young age on pavements, dams, concrete slabs of composite structures, massive parts poured in successive layers, etc., for which the *E*-modulus, and more importantly its evolution in time, is one of the most critical material-to-structural mechanical design parameters affecting the likelihood of early-age concrete cracking (see reviews by, e.g., Refs. [1–3]). The *E*-modulus, in effect, evolves substantially with the hardening of the material and increases continuously from zero to a value near its service value.

It has long been recognized that this early-age concrete stiffening, which is often referred to as 'aging elasticity,' cannot be described as a simple function of time. In fact, the kinetics of this stiffening is related to the hydration reactions of the material, which are thermally activated. This brought about macroscopic approaches, in which the evolution of the *E*-modulus was described by the maturity concept [4–8] or the hydration degree [9–12] or the solidification degree [13]. It has been shown that the maturity degree and the hydration degree are thermodynamically equivalent macroscopic state variables [14]. The hydration degree concept has been widely used in many large-scale engineering applications, ranging from innovative bridge design [15,16], shotcrete tunnel engineering [17–19], to concrete dam engineering [20,21].

Still, the macroscopic hydration degree concept is only a first step towards a comprehensive materials-to-

* Corresponding author. Tel.: +1-617-253-3544; fax: +1-617-253-6044.
E-mail address: ulm@mit.edu (F.-J. Ulm).
URL: http://cist.mit.edu.

0008-8846/03/$ – see front matter © 2003 Elsevier Ltd. All rights reserved.
doi:10.1016/S0008-8846(03)00039-5

structural engineering design approach, which aims at optimizing the structural performance of early-age concrete structures by means of an appropriate material choice. Recent progress in experimental mechanics, particularly in nanoindentation techniques, makes it possible to assess the elastic properties at very fine scales [22,23] and to upscale this elastic behavior to larger scales by means of advanced homogenization methods: cement paste [23], mortar, and concrete [24–27]. To our knowledge, this approach has been only employed for hardened cement-based materials, and there is still a missing link between the physical chemistry of cement hydration and the micro- to macromechanics of cement-based materials.

The goal of this paper is to close this gap by modeling the aging elasticity of early-age concrete composites. The originality of the proposed approach relies on use of a multistep micromechanical homogenization procedure that starts at the nanolevel of the C–S–H matrix, along with a physical chemistry model for the kinetics of the four main hydration reactions of ordinary portland cement (OPC) that determine the volume fractions of the involved mechanically active phases.

2. Elements of continuum micromechanics

Concrete is a fairly complex heterogeneous composite material, with a random microstructure at different length scales ranging from the nanometer scale to the macroscopic decimeter scale. Continuum micromechanics offers a framework to address this heterogeneity. The underlying idea of continuum micromechanics is that it is possible to separate a heterogeneous material into phases with on-average constant material properties. The three elements of continuum micromechanics are (see, e.g., Ref. [28]):

1. Representation, which deals with the geometrical description of the considered heterogeneous material system. Representation includes the identification of the different phases in a representative element volume V (r.e.v.), and their morphology. A phase, in the sense of continuum micromechanics, is not necessarily a material phase as used in physical chemistry, but a material domain that can be identified at a given scale with a homogeneous deformation state that is with constant material properties.
2. Localization, which establishes the link between a microscopic on-average constant strain (or stress state), prescribed at the boundary ∂V of the r.e.v., and the strain state (or stress state) in the individual (homogeneous) phases composing the r.e.v.
3. Homogenization, which is based on volume averaging over the r.e.v. of the constitutive relations defined at the scale of the phases. Homogenization delivers the macroscopic properties of the r.e.v. as a function of the microscopic phase properties, their volume fractions, and their specific morphologies.

Application of these three elements to cement-based materials at early ages is detailed below.

2.1. Representation of the multiscale microstructure of early-age concrete

The heterogeneity of cement-based material manifests itself at different scales. For purpose of mechanical analysis, the microstructure can be broken down into four elementary levels, as sketched in Fig. 1 [23]:

1. The lowest level (Level I) we consider is the one of the C–S–H matrix that forms at early ages by the hydration of C_3S and C_2S.[1] This level of a characteristic length scale of 10^{-8}–10^{-6} m is the smallest material length scale that is, at present, accessible by mechanical testing, i.e., nanoindentation. For this reason, lower scales, which are investigated by, e.g., quasi-elastic neutron scattering [29], will not be considered here. At the considered Level I, it now well established that the C–S–H exist in at least two different forms with different volume fractions [30] and elastic properties [22,23]. The morphology of the two types of C–S–H is correlated with two different processes of hydration of clinker compounds. During the early stages of hydration, nucleation and growth of C–S–H occurs at the surface of the cement grains, leading to the softer outer products. With hydration progressing (t>20 h for C_3S, see Ref. [31], for temperature effect, see, e.g., Ref. [29]), the cement grains are covered by a growing layer of C–S–H, and the hydration is controlled by the diffusion process through this layer. While outer products are still formed, new C–S–H is primarily formed in a space confined by the existing C–S–H layer; and these new C–S–H have a higher density, leading to an on-average higher stiffness of the inner product C–S–H. Many labels have been devised in cement chemistry for the two types of C–S–H in cement-based materials: OP–C–S–H and IP–C–S–H for Outer and Inner Products [32–34], Middle Product and Late Product [35,36], Groundmass and Phenograins [37], or more recently LD–C–S–H and HD–C–S–H for low-density and high-density C–S–H [30,38]. From a mechanical point of view, however, only average stiffness values of these two types of C–S–H are accessible by nanoindentation, that is, mean stiffness values for low-density and high-density C–S–H [23], which include the nanoporosity (or C–S–H gel porosity) and eventually some fine calcium hydroxide crystals intimately mixed with the gels. We refer to these two types of C–S–H as

[1] The cement's chemistry abbreviations will be used in this paper (C_3S=3CaO·SiO_2, C_2S=2CaO·SiO_2, C_3A=3CaO·Al_2O_3, C_4AF=4CaO·Al_2O_3·Fe_2O_3).

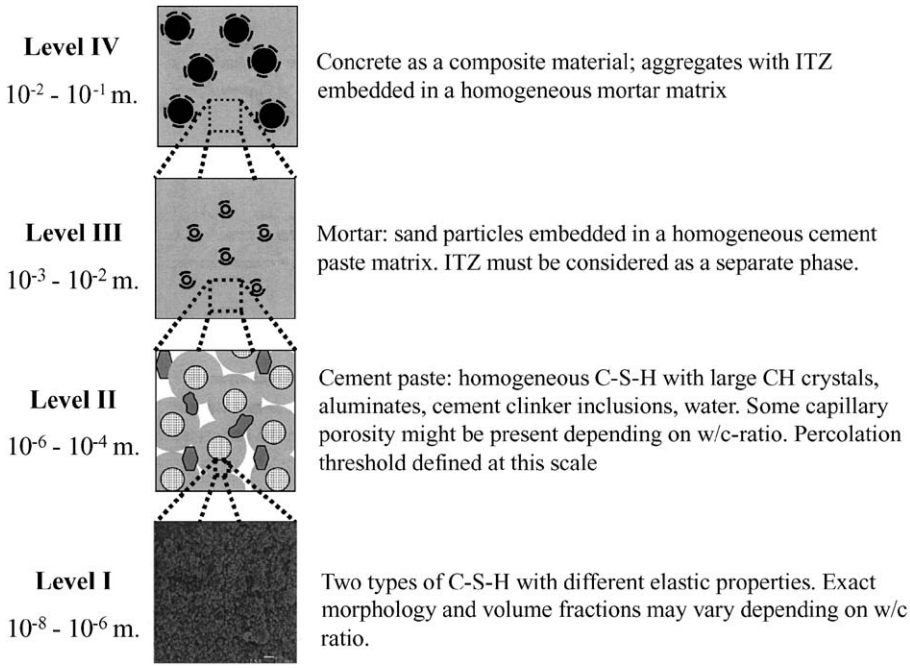

Fig. 1. Multiscale microstructure of cement-based materials, adapted from Ref. [23].

phases in a micromechanical sense, as detailed before; that is, each C–S–H phase is associated with a homogeneous deformation state and homogeneous mechanical properties. This mechanical definition of the C–S–H phases, which is consistent with the nanoindentation results, justifies the use of a neutral labeling of these two types of C–S–H phases as C–S–H_a phase and C–S–H_b phase, associated, respectively, with the outer and inner products, or low-density and high-density products. From a morphological point of view, the C–S–H matrix can be considered as a two-phase material, composed of a stiffer inclusion phase (C–S–H_b phase) embedded into a softer matrix phase (C–S–H_a phase). At early ages, the volume fractions of these two phases depend on the progress of the C_3S and C_2S–clinker hydration. This level is the starting point for the homogenization approach developed in this paper.

2. The C–S–H matrix, together with unhydrated cement products (i.e., the four clinker phases C_3S, C_2S, C_3A, C_4AF), large portlandite crystals (CH=$Ca(OH)_2$), aluminates (see exact formulations in Ref. [35]), and macroporosity in the case of high water-to-cement ratio materials (roughly w/c>0.4 [39]) forms the cement paste and is referred to as Level II (10^{-6}–10^{-4} m). At early ages, it is the scale of the solid percolation threshold. More precisely, when OPC is mixed with water, the solid phases (clinker) of the composite material are discontinuous. The freshly mixed material can be considered as a pure viscous liquid with nonappreciable shear modulus [40]. The solid phase is then built up through random growth of hydration products, mainly due to the formation of C–S–H at the surface of cement grains. Once the solid phases become connected, the composite material at level II can support appreciable shear stresses. Following percolation theory, this set point is generally referred to as the solid percolation threshold [41,42]. At the micrometer scale, this percolation threshold is considered to be a material property that is mainly affected by the w/c ratio and the cement fineness. It is one focus of this paper to derive this percolation threshold from micromechanics theory. More precisely, from a morphological point of view, a transformation occurs during hydration from a highly disordered microstructure without any phase dominating, to a matrix-inclusion morphology. Once the C–S–H phase percolates, the composite cement paste consists of inclusions (clinker phases, A-phase, CH phase and porosity) embedded into a C–S–H matrix.
3. Level III (10^{-3}–10^{-2} m) refers to mortar; that is a three-phase composite material composed of a cement paste matrix, sand particle inclusions, and an interfacial transition zone (ITZ). This scale has been focus of micromechanical modeling attempts, both analytically (e.g., Refs. [27,43]) and numerically (e.g., Refs. [26,42]). For early-age concrete, there is a critical lack of data concerning the development of mechanical properties of the ITZ; related, e.g., to a higher CH concentration. In this paper, in a first approach, we will not consider the ITZ, but will reduce the three-phase composite material to a two-phase material composed of spherical inclusions of sand particles (<2 mm) embedded in a continuous matrix of homogenized cement paste. In this case, the important volume fractions are those of the inclusion and of the matrix, and they are fixed in time.

4. Concrete as a composite material is considered on Level IV (10^{-2}–10^{-1} m). Similar to Level III, homogenization approaches that consider at this scale a three-phase material composed of aggregates (>2 mm) embedded in a continuous homogeneous mortar matrix and an ITZ have been developed [42,43]. For early-age concrete, we restrict the analysis to a two-phase system composed of aggregates and mortar, and the required volume fractions are also fixed in time.

It is worth noting that the four levels described above respect the separability of scale condition; that is, each scale is separated by the next one by at least one order of length magnitude. This is a prerequisite for the application of continuum micromechanics [28].

2.2. Localization

The breakdown of the multiscale heterogeneous microstructure of cement-based materials into the four-level microstructure, separated on average by one or several order of length magnitude, allows us to consider each level as r.e.v., V, composed of n homogeneous phases (in a micromechanical sense) of constant material properties per phase, and volume fraction $f_r=V_r/V$, such that $\sum_{r=1,n} f_r=1$. Following continuum micromechanics, each level is considered to be subjected to a macroscopic strain prescribed at the boundary ∂V of the r.e.v. This homogeneous boundary condition, which is often referred to as Hashin-type boundary condition, reads:

$$\text{on } \partial V \ : \ \underline{u}(\underline{x}) = \underline{\underline{E}} \cdot \underline{x} \tag{1}$$

where $\underline{u}$ is the microscopic displacement vector, $\underline{x}$ denotes the position vector at the microscopic scale, and $\underline{\underline{E}}$ is the macroscopic strain tensor in V; the symbol "·" stands for scalar product. The macroscopic strain tensor $\underline{\underline{E}}$ is related to the microscopic strain $\underline{\underline{\varepsilon}}(\underline{x})$ by the volume-averaging relation:

$$\underline{\underline{E}} = \langle \underline{\underline{\varepsilon}}(\underline{x}) \rangle_V = \frac{1}{V} \int_V \underline{\underline{\varepsilon}}(\underline{x}) \mathrm{d}V \tag{2}$$

It is assumed in linear continuum micromechanics that the macroscopic strain $\underline{\underline{E}}$ can be linked to the microscopic strain $\underline{\underline{\varepsilon}}_r$ by means of a linear strain localization condition:

$$\underline{\underline{\varepsilon}}_r = \mathrm{A}_r \ : \ \underline{\underline{E}} \tag{3}$$

where A_r is a fourth-order localization or concentration tensor (as it concentrates a macroscopic quantity prescribed at the boundary into a microscopic phase), which obeys to the consistency condition (combination of Eqs. (2) and (3)):

$$\underline{\underline{E}} = \langle \underline{\underline{\varepsilon}}_r \rangle_V = \langle \mathrm{A}_r \ : \ \underline{\underline{E}} \rangle_V \Longleftrightarrow \langle \mathrm{A}_r \rangle_V = \mathrm{I} \tag{4}$$

The symbol ":" stands for double contraction. I is the fourth-order unit tensor. The simplest form of strain localization is a constant strain in all phases, that is, $\underline{\underline{\varepsilon}}_r=\underline{\underline{E}} \Longleftrightarrow \mathrm{A}_r=\mathrm{I}$, which forms the basis of so-called mixture theories. This localization condition, however, fails to describe the different strain distribution in the microstructure, which depends on stiffness and morphology of the different phases. In a refined approach, the strain localization tensor is estimated from the linear elastic solution of some idealized geometrical configurations. The most common one that applies best to the morphology encountered at all different levels of cement-based materials, is the Eshelbian-type ellipsoidal inclusion embedded in a reference medium [44], for which an estimate $\mathrm{A}_r^{\mathrm{est}}$ of the localization tensor is given in the form [28]:

$$\mathrm{A}_r^{\mathrm{est}} = [\mathrm{I} + \mathrm{S}_r^{\mathrm{Esh}} \ : \ (\mathrm{C}_0^{-1} \ : \ \mathrm{C}_r - \mathrm{I})]^{-1} \\ : \ \langle [\mathrm{I} + \mathrm{S}_r^{\mathrm{Esh}} \ : \ (\mathrm{C}_0^{-1} \ : \ \mathrm{C}_r - \mathrm{I})]^{-1} \rangle_V^{-1} \tag{5}$$

where C_0 is the tensor of elastic moduli of the reference medium, C_r is the fourth-order elasticity tensor of phase r=1,n, and $\mathrm{S}_r^{\mathrm{Esh}}$ is the Eshelby tensor of phase r, which depends on C_0, the geometry, and the orientation of phase r. Given the random microstructure of cement-based materials, it is naturally to consider all phases as isotropic and the inclusions as spherical. The first assumption implies the isotropy of the local and the reference medium, that is:

$$\mathrm{C}_r = 3k_r\mathrm{J} + 2\mu_r\mathrm{K}; \qquad \mathrm{C}_0 = 3k_0\mathrm{J} + 2\mu_0\mathrm{K} \tag{6}$$

where k_r, μ_r, k_0, and μ_0 are the bulk moduli and the shear moduli of phase r and of the reference medium, respectively; $J_{ijkl}=(1/3)\delta_{ij}\delta_{kl}$ is the volumentric part of the fourth-order unit tensor I, and K=I−J is the deviator part; δ_{ij} stands for the Kronecker delta. The second assumption of spherical inclusions implies the following form of the Eshelby tensor $\mathrm{S}_r^{\mathrm{Esh}}$ for phase r:

$$\mathrm{S}_r^{\mathrm{Esh}} = \alpha_0^{\mathrm{est}}\mathrm{J} + \beta_0^{\mathrm{est}}\mathrm{K} \tag{7}$$

with

$$\alpha_0^{\mathrm{est}} = \frac{3k_0}{3k_0 + 4\mu_0}; \qquad \beta_0^{\mathrm{est}} = \frac{6(k_0 + 2\mu_0)}{5(3k_0 + 4\mu_0)} \tag{8}$$

2.3. Homogenization and choice of reference medium

To homogenize the local material properties, constitutive relations are required for the different phases, together with the volume-averaging relation linking the microscopic stress $\underline{\underline{\sigma}}_r$ and the macroscopic stress $\underline{\underline{\Sigma}}$; analogously to Eq. (2):

$$\underline{\underline{\Sigma}} = \langle \underline{\underline{\sigma}}(\underline{x}) \rangle_V \tag{9}$$

Use in Eq. (9) of a linear elastic constitutive law for each microscopic phase, i.e., of the form $\underline{\underline{\sigma}}_r=\mathrm{C}_r \ : \ \underline{\underline{\varepsilon}}_r$, together with the strain localization condition (Eq. (3)),

i.e., $\underline{\underline{\sigma}}_r=(C_r : A_r) : \underline{\underline{E}}$, delivers the following linear homogenization formula for the macroscopic (or homogenized) elasticity tensor C_{hom}:

$$\underline{\underline{\Sigma}} = C_{hom} : \underline{\underline{E}};\ C_{hom} = \langle C_r : A_r \rangle_V = \sum_r f_r C_r : A_r \quad (10)$$

While expression (10) is an exact theoretical definition of C_{hom}, the practical determination of C_{hom} is generally based on estimates of the localization tensor for each phase A_r^{est}. It is readily understood that the quality of the homogenization result is intimately related to the quality of the localization condition. For instance, use of $A_r^{est}=I$ (which comes to assume the same strain in all phases and macroscopically) delivers the Voigt upper bound (or mixture rule),

$$\forall r, A_r^{est} = I, C_{hom}^{est} = \langle C_r : I \rangle_V = \sum_r f_r C_r \quad (11)$$

In a refined analysis, considering the Eshelbian-type strain localization (Eq. (5)), the following estimate of the macroscopic (or homogenized) elasticity tensor C_{hom}^{est} is obtained:

$$C_{hom}^{est} = \langle C_r : [I + S_r^{Esh} : (C_0^{-1} : C_r - I)]^{-1} \rangle_V : \langle [I + S_r^{Esh} : (C_0^{-1} : C_r - I)]^{-1} \rangle_V^{-1} \quad (12)$$

Substituting Eqs. (6)–(8) into Eq. (12) yields explicit expressions for the homogenized bulk modulus and shear modulus:

$$C_{hom}^{est} = 3k_{hom}^{est} J + 2\mu_{hom}^{est} K \quad (13)$$

$$k_{hom}^{est} = \sum_r f_r k_r \left(1 + \alpha_0^{est}\left(\frac{k_r}{k_0} - 1\right)\right)^{-1} \times \left[\sum_r f_r \left(1 + \alpha_0^{est}\left(\frac{k_r}{k_0} - 1\right)\right)^{-1}\right]^{-1} \quad (14)$$

$$\mu_{hom}^{est} = \sum_r f_r \mu_r \left(1 + \beta_0^{est}\left(\frac{\mu_r}{\mu_0} - 1\right)\right)^{-1} \times \left[\sum_r f_r \left(1 + \beta_0^{est}\left(\frac{\mu_r}{\mu_0} - 1\right)\right)^{-1}\right]^{-1} \quad (15)$$

To close the upscaling procedure, we need to choose the appropriate reference medium, in which the inclusions are embedded. This choice is important as it determines the level of interaction between inclusions and special physical features such as the percolation threshold that are taken into account in the localization and homogenization procedure. For the four-level upscaling procedure, we consider:

(1) The Mori–Tanaka scheme [45], in which the matrix phase is chosen as reference medium, i.e., $C_0 \equiv C_m$. The MT scheme is appropriate for materials that exhibit a strong matrix-inclusion morphology and mechanical interactions in between particles. This scheme is chosen for the two-phase spherical inclusion composites at Level I, Level III, and Level IV, for which Eqs. (14) and (15) reduce to:

$$\frac{k_{hom}^{est}}{k_m} = 1 + f_I \frac{k_I/k_m - 1}{1 + \alpha_m^{est}(1 - f_I)(k_I/k_m - 1)} \quad (16)$$

$$\frac{\mu_{hom}^{est}}{\mu_m} = 1 + f_I \frac{\mu_I - \mu_m}{1 + \beta_m^{est}(1 - f_I)(\mu_I/\mu_m - 1)} \quad (17)$$

and Eq. (8) to:

$$\alpha_0^{est} \equiv \alpha_m^{est} = \frac{3k_m}{3k_m + 4\mu_m}; \qquad \beta_0^{est} \equiv \beta_m^{est} = \frac{6(k_m + 2\mu_m)}{5(3k_m + 4\mu_m)} \quad (18)$$

(2) The self-consistent scheme [46,47], in which the reference medium coincides with the homogenized medium, $C_0 \equiv C_{hom}^{est}$. The SCS describes well materials characterized by perfect disorder (polycrystal). Being related to percolation theory, it allows one to account for a percolation threshold. The SCS, therefore, is chosen for Level II homogenization to account for a solid percolation threshold. In contrast to the MT scheme, the SCS involves the solution of two nonlinear equations (Eqs. (14) and (15)), in which $k_0 \equiv k_{hom}^{est}$; $\mu_0 \equiv \mu_{hom}^{est}$.

Finally, for the purpose of comparison with experimental data, the homogenized Young's modulus and Poisson's ratio at each level are evaluated from:

$$E_{hom}^{est} = \frac{9k_{hom}^{est}\mu_{hom}^{est}}{3k_{hom}^{est} + \mu_{hom}^{est}};\ \nu_{hom}^{est} = \frac{3k_{hom}^{est} - 2\mu_{hom}^{est}}{6k_{hom}^{est} + 2\mu_{hom}^{est}} \quad (19)$$

3. Input parameters

The four-level upscaling scheme requires, at each level, input of the shear and bulk moduli, $k_{r=1,n}$ and $\mu_{r=1,n}$, and of the volume fractions of the involved phases, $f_{r=1,n}$. The output, k_{hom}^{est} and μ_{hom}^{est}, at each level serves as the input for the next level. Table 1 summarizes the input–output structure of the four-level upscaling scheme. The mechanical, chemical, and mix-design input parameters are detailed below.

Table 1
Input–output structure of the four-level upscaling scheme

Level	Input			Output
	Mechanical	Chemical	Mix-Design	
I: C–S–H matrix				MT scheme
C–S–H_a	k_a, μ_a	f_a		k^{est}_{C-S-H}, μ^{est}_{C-S-H}
C–S–H_b	k_b, μ_b	$f_b=1-f_a$		
II: Cement paste				SCS scheme
C–S–H matrix	k^{est}_{C-S-H}, μ^{est}_{C-S-H}	f_{C-S-H}		k^{est}_{CP}, μ^{est}_{CP}
C_3S–Clinker	k_{C_3S}, μ_{C_3S}	f_{C_3S}		
C_2S–Clinker	k_{C_2S}, μ_{C_2S}	f_{C_2S}		
C_3A–Clinker	k_{C_3A}, μ_{C_3A}	f_{C_3A}		
C_4AF–Clinker	k_{C_4AF}, μ_{C_4AF}	f_{C_4AF}		
CH	k_{CH}, μ_{CH}	f_{CH}		
Aluminates	k_A, μ_A	f_A		
Water	–	f_w		
Voids	–	f_v		
III: Mortar				MT scheme
CP–matrix	k^{est}_{CP}, μ^{est}_{CP}		$f_{CP}=1-f_s$	k^{est}_{M}, μ^{est}_{M}
Sand (<2 mm)	k_s, μ_s		f_s	
IV: Concrete				MT scheme
Mortar-matrix	k^{est}_{M}, μ^{est}_{M}		$f_M=1-f_g$	k^{est}_{C}, μ^{est}_{C}
Aggregate (>2 mm)	k_g, μ_g		f_g	

3.1. Mechanical input parameters: nanoindentation data

Recent progress in instrumented nanoindentation provides a fairly consistent amount of data for the mechanical input parameters of the model (see Table 2):

- Level I: Acker [22] and Constantinides and Ulm [23] provided values for the mean elastic stiffness of the two C–S–H phases at Level I. The values, which were obtained for two different types of cement pastes and with different sharp indenters, coincide, suggesting that the values are intrinsic material parameters that do not depend on mix proportioning. That what differs, at this scale, from one cement paste to another is the volume fraction of the two phases, which depends on the mix proportioning. Given the scale which is accessible by nanoindentation, the stiffness value for each C–S–H phase includes both the solid phase and the nanoscale gel porosity within the C–S–H.
- Level II: Beaudoin [48] and Wittmann [49] measured the elastic modulus of CH compacts on specimens with different porosities. The elastic modulus of these compacts was obtained from three-point bending tests. The intrinsic modulus of CH was found by extrapolating to zero porosity, log$E$ versus porosity curves. The order of magnitude of these values was confirmed by nanoindentation results by Acker [22] and Constantinides and Ulm [23], which also lie within the bounds determined by Monteiro and Chang [50]. The stiffness of the clinker phases (C_3S, C_2S, C_3A, C_4AF) were determined by indentation by Acker [22] and by extrapolation techniques by Velez et al. [51]. Unfortunately, there is a lack of data on the elastic properties of aluminates. It is reasonable to assume that these properties are similar to the elastic properties of the C–S–H matrix, obtained by the first-level upscaling procedure.
- Levels III and IV: The elastic stiffness of sand and aggregates are well known (see for instance Ref. [52]) and are typically provided by the aggregate supplier.

These mechanical input parameters are considered to be time independent.

3.2. Chemical input parameters

The second set of input parameters is the set of volume fractions occupied by the different phases in the r.e.v. at Level I and Level II. Given that the phases form via the four elementary hydration reactions, it is natural to determine the volume fractions from cement chemistry. This requires two steps: (1) determination of the hydration degree of each reaction from reaction kinetic laws and (2) consideration of the volume change associated with each reaction.

3.2.1. Hydration kinetics model

It is common practice in physical chemistry (see, e.g., Atkins [53]) to describe the kinetics of hydration of each clinker phase X (X=C_3S, C_2S, C_3A, and C_4AF) by nucleation and growth kinetic laws that link the reaction rate $d\xi_X/dt$ to the driving force for the chemical reaction, called the affinity

Table 2
Intrinsic elastic properties of cement paste constituents

Level	E (GPa)	ν (–)	References
I: C–S–H matrix			
C–S–H_a	20±2		Acker [22]
	21.7±2.2	**0.24**	Constantinides and Ulm [23]
C–S–H_b	31±4		Acker [22]
	29.4±2.4	**0.24**	Constantinides and Ulm [23]
II: Cement paste			
C_3S–Clinker	**135±7**	**0.3**	Acker [22]
	147±5	**0.3**	Velez et al. [51]
C_2S–Clinker	**140±10**	**0.3**	Acker [22]
	130±20	**0.3**	Velez et al. [51]
C_3A–Clinker	160±10		Acker [22]
	145±10		Velez et al. [51]
C_4AF–Clinker	**125±25**		Velez et al. [51]
CH	35.24		Beaudoin [48]
	48		Wittmann [49]
	39.77–44.22	**0.305**–0.325	Monteiro and Chang [50]
	36±3		Acker [22]
	38±5		Constantinides and Ulm [23]

Values in bold are used in the homogenization procedure.

Table 3
Reaction kinetic model parameters of the four clinker hydration reactions (from Refs. [31,35])

Clinker	*w/c*	Avrami model			Diffusion model		Activation energy $E_{aX}/\mathscr{R}$ [K]
		$\tau_X(T_0)$ [h]	κ [1]	$\xi_{X,0}$ [1]	D [cm^2/h]	ξ_X^* [1]	
C_3S	0.3	13.5	1.86	0.02	0.42×10^{-10}	0.60	4500
	0.5	11.9	1.72		2.64×10^{-10}		
	0.7	10.5	1.66		15.6×10^{-10}		
C_2S	0.3	71.2	1.10	0.00	6.64×10^{-13}	0.60	2500
	0.5	60.9	0.96				
	0.7	58.6	0.84				
C_3A	0.3	57.7	1.14	0.04	2.64×10^{-10}	0.60	5500
	0.5	49.2	1.00				
	0.7	35.9	0.86				
C_4AF	0.3	27.0	2.44	0.40	0.42×10^{-10}	0.60	4200
	0.5	21.4	2.30		2.64×10^{-10}		
	0.7	14.3	2.16		15.6×10^{-10}		

Values for other *w/c* ratio are linearly interpolated.

$A(\xi_X)$, in addition to any kinetics constant that determines the time scale of the chemical reaction. These kinetic laws can be written in the following dimensionless form:

$$\tau_X \frac{d\xi_X}{dt} = \tilde{A}(\xi_X) \tag{20}$$

where τ_X is the characteristic time associated with the reaction, and $\tilde{A}(\xi_X)$ is a normalized affinity. Given the thermal activation of the hydration reaction, the characteristic time depends on the temperature, and this dependency is well described, for cement hydration, by the Arrhenius concept:

$$\tau_X(T) = \tau_X(T_0)\exp\left[\frac{E_{aX}}{\mathscr{R}}\left(\frac{1}{T_0}-\frac{1}{T}\right)\right] \tag{21}$$

where E_{aX} is the activation energy of the chemical reaction, $\mathscr{R}$ the universal gas constant, and $\tau_X(T_0)$ is the characteristic time of the reaction at a constant reference temperature T_0 (typically, T_0=293 K). The expression of the normalized affinity depends on the physical process at stake. For the cement hydration, there are (at least) three processes [35].

(1) Dissolution of the clinker phases during the induction period. Given the relatively short period, the process can be simulated by a constant reaction rate; that is, $\tilde{A}$=1 and $\tau_X=\tau_{X,0}=t_{X,0}/\xi_{X,0}$, where $t_{X,0}$ is the duration of the induction period, and $\xi_{X,0}$ is the degree of hydration threshold of clinker X at the end of the induction period.

(2) Nucleation and growth-controlled hydration of the clinker phases, which is the focus of, e.g., the Avrami model [54], commonly employed in cement chemistry. Expressed in the form of the kinetic law (Eq. (20)), the normalized affinity of the Avrami model reads (see derivation in Appendix):

$$\tilde{A}^A(\xi_X) = \frac{(1-\delta\xi_X)}{(-\ln(1-\delta\xi_X))^{\frac{1}{\kappa}-1}} \quad \text{for}$$

$$\delta\xi_X = \langle \xi_X - \xi_{X,0}\rangle_+ > 0 \tag{22}$$

and the characteristic time:

$$\tau_X(T_0) = \frac{1}{\kappa k} \tag{23}$$

where $\langle x\rangle_+$ denotes the positive part of x. The exponent κ defines the reaction order, and k is the rate constant. The Avrami parameters, κ, and $\xi_{X,0}$, together with the kinetic parameters $\tau_X(T_0)$ and $E_{aX}/\mathscr{R}$, are well established by now (see, e.g., Berliner et al. [31]), even though some coefficients may vary from one author to the other (see also Ref. [55]). The values used in this paper are taken from Ref. [31] and are summarized in Table 3.

(3) Beyond a critical hydration degree ξ_X^*, which corresponds to a critical thickness of hydration products formed around the clinker grains, the kinetics of the hydration reactions is limited by diffusion of dissolved ions through the layers of hydrates formed around the clinker. The problem has been addressed by several authors by means of diffusion theory [31,56]. We refer to the works of Fuji and Kondo [56]. Written in the rate form of kinetic law (Eq. (20)), the normalized affinity of this process can be expressed as:

$$\tilde{A}^D(\xi_X) = \frac{(1-\xi_X)^{\frac{2}{3}}}{(1-\xi_X^*)^{\frac{1}{3}}-(1-\xi_X)^{\frac{1}{3}}} \quad \text{for } \xi_X > \xi_X^* \tag{24}$$

and the characteristic time by:

$$\tau_X(T_0) = \frac{R^2}{3D} \tag{25}$$

where D is a diffusion coefficient (of dimension $[D]=L^2/T$), and R is the average initial radius of clinker grains. The model parameters, ξ_X^* and D, of the diffusion-type kinetics law of the different clinker phases are extracted from the works of Berliner et al. [31] and Taylor [35]. They are summarized in Table 3.

The values of the kinetic parameters in Table 3 have been determined for an OPC of a fineness ϕ_0=3602 cm^2/g and an average particle size $R=5\times10^{-4}$ cm. Given that the hydra-

Table 4
Input parameters for the determination of the volume fractions (level I and level II)

	Reactants						Products	
	C_3S	C_2S	C_3A	C_4AF	w	c	C–S–H	CH
$\rho_X^{(*)}$ [g/cm^3]	$\rho_c \frac{m_{C_3S}}{\sum_X m_X}$	$\rho_c \frac{m_{C_2S}}{\sum_X m_X}$	$\rho_c \frac{m_{C_3A}}{\sum_X m_X}$	$\rho_c \frac{m_{C_4AF}}{\sum_X m_X}$	1.00	3.15	2.04	2.24
$\mathscr{M}_X$ [g/mol]	228.32	172.24	270.20	430.12	18	–	227.2	74
θ^X_{C-S-H} [1]	1.0	1.0	–	–	–	–	–	–
θ^X_{CH} [1]	1.3	0.3	–	–	–	–	–	–
θ^X_w [1]	5.3	4.3	10.0	10.75	–	–	–	–
θ^X_V [1]	−0.073	−0.077			–	–	–	–

tion kinetics is accelerated by a smaller fineness due to the greater specific surface area, the values of the characteristic time determined from Eq. (25) are corrected by:

$$\tau_X(T_0,\phi) = \frac{\phi_0}{\phi} \times \tau_X(T_0,\phi_0) \tag{26}$$

The hydration kinetics model is then complete.

Finally, it is useful to recall the relation between the clinker hydration degrees ξ_X and the overall hydration degree $\xi(t)$ of cement-based material systems [57,35]:

$$\xi(t) = \frac{\sum_X m_X \xi_X(t)}{\sum_X m_X} \tag{27}$$

where m_X=m_{C_3S}, m_{C_2S}, m_{C_3A}, and m_{C_4AF} are the mass fractions of the clinker phases in the cement, which are generally provided by the cement producer, based on a chemical analysis of the cement (see, e.g., Taylor [35]). For instance, the mass fraction of C_3S in OPC is typically $m_{C_3}S$=0.6.

3.2.2. Volume fractions Level I

The hydration kinetics model determines the hydration degree of each clinker phase, which is required for the determination of the volume fractions of the phases involved in the micromechanics model. At Level I, the two types of C–S–H are the reaction products of the hydration of C_3S and C_2S. If we accept that the low-density C–S–H_a phase corresponds to the outer products, and the high-density C–S–H_b phase to the inner products, it is natural to assume that the first are formed during the nucleation and growth process ($\xi_X \le \xi_X^*$), and the second during the diffusion-controlled hydration reaction, that is:

$$V_a(t) = V^{C_3S}_{C-S-H}(\xi^*_{C_3S} - \langle \xi^*_{C_3S} - \xi_{C_3S}(t)\rangle_+) + V^{C_2S}_{C-S-H}(\xi^*_{C_2S} - \langle \xi^*_{C_2S} - \xi_{C_2S}(t)\rangle_+) \tag{28}$$

$$V_b(t) = V^{C_3S}_{C-S-H}\langle \xi_{C_3S}(t) - \xi^*_{C_3S}\rangle_+ + V^{C_2S}_{C-S-H}\langle \xi_{C_2S}(t) - \xi^*_{C_2S}\rangle_+ \tag{29}$$

where $V^{C_3S}_{C-S-H}$ and $V^{C_2S}_{C-S-H}$ are asymptotic values of the volume occupied by the reaction products of the hydration of C_3S and C_2S in the C–S–H r.e.v. V_{C-S-H}=$V^{C_3S}_{C-S-H}$+$V^{C_2S}_{C-S-H}\cdot V^{C_3S}_{C-S-H}$ (resp. $V^{C_2S}_{C-S-H}$) can be determined in a dimensionless form from:

$$\frac{V^{C_3S}_{C-S-H}}{V^0_c} = \theta^{C_3S}_{C-S-H} \times \frac{\rho^*_{C_3S}/\mathscr{M}_{C_3S}}{\rho_{C-S-H}/\mathscr{M}_{C-S-H}};$$

$$\rho^*_{C_3S} = \frac{M_{C_3S}}{V^0_c} = \rho_c \frac{m_{C_3S}}{\sum_X m_X} \tag{30}$$

$$\frac{V^{C_2S}_{C-S-H}}{V^0_c} = \theta^{C_2S}_{C-S-H} \times \frac{\rho^*_{C_2S}/\mathscr{M}_{C_2S}}{\rho_{C-S-H}/\mathscr{M}_{C-S-H}};$$

$$\rho^*_{C_2S} = \frac{M_{C_2S}}{V^0_c} = \rho_c \frac{m_{C_2S}}{\sum_X m_X} \tag{31}$$

where $\theta^{C_3S}_{C-S-H}$=n_{C-S-H}/n_{C_3S} =1 and $\theta^{C_2S}_{C-S-H}$=n_{C-S-H}/n_{C_2S}= 1 express that n_{C_3S} =1 mol of C_3S (resp. n_{C_2S} =1 mol of C_2S) is required for the formation of n_{C-S-H}=1 mol of C–S–H; V^0_c is the initial cement volume, $\rho^*_{C_3S}$ (resp. $\rho^*_{C_2S}$) is the apparent mass density of C_3S (resp. C_2S) in cement (mass density ρ_c); $\mathscr{M}_{C_3S}$, $\mathscr{M}_{C_2S}$=molar mass of C_3S and C_2S, such that $\rho^*_{C_3S}/\mathscr{M}_{C_3S}$=number of moles of C_3S per unit volume of cement, and analogously, $\rho_{C-S-H}/\mathscr{M}_{C-S-H}$=number of moles of C–S–H per unit volume of C–S–H (ρ_{C-S-H}=mass density of C–S–H; $\mathscr{M}_{C-S-H}$=molar mass of C–S–H). The input values for the determination of $V^{C_3S}_{C-S-H}$ and $V^{C_2S}_{C-S-H}$ are given in Table 4.

Finally, the relative volume fractions at level I of the two types of C–S–H are then obtained from:

$$f_a = \frac{V_a}{V_a + V_b}; \qquad f_b = \frac{V_b}{V_a + V_b} = 1 - f_a \tag{32}$$

Fig. 2 displays, as a function of the hydration degree, ξ, the evolution of the volume fractions of the two types of C–S–H for a w/c=0.5 cement paste. At complete hydration (ξ=1), the model predicts $f_a \approx 0.7$ and $f_b \approx 0.3$, which is in perfect agreement with the volume fractions determined analytically by Tennis and Jennings [30] based on specific surface measurements and experimentally by Constantinides and

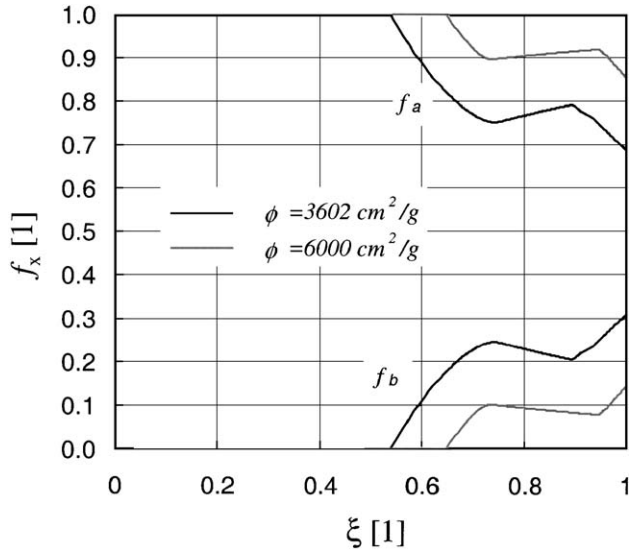

Fig. 2. Influence of the cement fineness on the evolution of the volume fractions of the two types of C–S–H phases for a w/c=0.5 OPC paste (Level I).

Ulm [23] based on a statistical analysis of nanoindentation results. The evolution of the two types of C–S–H for a finer cement (ϕ=6000 cm^2/g) are also presented in Fig. 2. In such conditions, the volume fraction of C–S–H_b is divided by 2 at the end of the hydration.

3.2.3. Volume fractions Level II

Level II is composed of both reactants and products. On the reactant side, the volume occupied by the four clinker phases is linearly related to the clinker hydration degree, that is:

$$V_X(t) = V_X^0(1-\xi_X(t)); \qquad \frac{V_X^0}{V_c^0} = \frac{m_X}{\sum_X m_X} \tag{33}$$

where V_X^0 is the initial volume of the clinker phases in the cement. The other reactant phase is water, which is consumed in the four hydration reactions:

$$V_w(t) = V_w^0 - \sum_X V_w^X \times \xi_X(t) \geq 0 \tag{34}$$

V_w^0 is the initial volume of water in the mix, and V_w^X is the volume of water that is consumed in the clinker hydration reaction (complete hydration), which is given by:

$$\frac{V_w^X}{V_c^0} = \theta_w^X \times \frac{\rho_X^*/\mathcal{M}_X}{\rho_w/\mathcal{M}_w}; \quad \rho_X^* = \frac{M_X}{V_c^0} = \rho_c \frac{m_X}{\sum_X m_X} \tag{35}$$

where $\theta_w^X = n_w/n_X$ denotes the number n_w of moles of water consumed during the hydration of n_X=1 mol of clinker phase X of apparent mass density ρ_X^*. For instance, in the hydration of n_{C_3S}=1 mol of C_3S, 4 mol of water are fixed by the formation of C–S–H (1.1 mol are chemically bound, 2.9 mol are absorbed in the C–S–H pores), and 1.3 mol of water are involved in the hydration of C_3S to form CH; thus, $\theta_w^{C_3S}$=(4+1.3)/1=5.3; analogously, $\theta_w^{C_2S}$=(4+0.3)/1=4.3; θ_w^{C3A}=10 and $\theta_w^{C_4AF}$=10.75; see Table 4.

On the product side, the volume occupied by the C–S–H matrix, $V_{C-S-H}=V_a+V_b$, is defined by Eqs. (28) and (29),

$$V_{C-S-H}(t) = V_{C-S-H}^{C_3S} \times \xi_{C_3S}(t) + V_{C-S-H}^{C_2S} \times \xi_{C_2S}(t) \tag{36}$$

where $V_{C-S-H}^{C_3S}$ and $V_{C-S-H}^{C_2S}$ are defined by Eqs. (30) and (31). Analogously, the volume occupied by the Portlandite, CH, is a combination of the reaction products of the hydration of C_3S and C_2S:

$$V_{CH}(t) = V_{CH}^{C_3S} \times \xi_{C_3S}(t) + V_{CH}^{C_2S} \times \xi_{C_2S}(t) \tag{37}$$

where $V_{CH}^{C_3S}$ and $V_{CH}^{C_2S}$ are the asymptotic volume contributions of the C_3S and C_2S hydration to the CH formation:

$$\frac{V_{CH}^{C_3S}}{V_c^0} = \theta_{CH}^{C_3S} \times \frac{\rho_{C_3S}^*/\mathcal{M}_{C_3S}}{\rho_{CH}/\mathcal{M}_{CH}};$$

$$\frac{V_{CH}^{C_3S}}{V_c^0} = \theta_{CH}^{C_2S} \times \frac{\rho_{C_2S}^*/\mathcal{M}_{C_2S}}{\rho_{CH}/\mathcal{M}_{CH}} \tag{38}$$

where $\theta_{CH}^{C_3S}=n_{CH}/n_{C_3S}$=1.3 (i.e, hydration of n_{C_3S}=1 mol of C_3S leads to the formation of n_{CH}=1.3 mol of CH); $\theta_{CH}^{C_2S}=n_{CH}/n_{C_2S}$=0.3, and $\rho_{CH}/\mathcal{M}_{CH}$=number of moles per unit volume of CH (ρ_{CH}=mass density of CH; $\mathcal{M}_{CH}$=molar mass of CH; see Table 4).

Finally, during the hydration of the clinker phases, capillary voids are created due to a negative volume balance (or chemical shrinkage) between reactant and product phases involved in the hydration reactions of the clinker phases:

$$V_V(t) = -\sum_X \Delta V_V^X \times \xi_X(t); \quad \frac{\Delta V_V^X}{V_c^0} = \theta_V^X \times \frac{m_X}{\sum_X m_X} \tag{39}$$

According to Taylor [35], $\theta_V^{C_3S}$=−0.073; $\theta_V^{C_2S}$= $\theta_V^{C_3A}$= $\theta_V^{C_4AF}$=−0.077; see Table 4.

The total volume of the r.e.v. at Level II is the sum of the volumes of both reactant and product phases, that is:

$$V_{II} = \underbrace{V_w(t) + \sum_X V_X(t)}_{\text{Reactants}} + \underbrace{V_{C-S-H}(t) + V_{CH}(t) + V_A(t) + V_V(t)}_{\text{Products}} \tag{40}$$

where $V_A(t)$ is the volume occupied by the aluminates. The volume of the r.e.v. is constant in time and can therefore be evaluated from the initial volume of the cement and water in the mixture:

$$V_{II} = V_c^0 + V_w^0 = V_c^0 \times \left(1 + \frac{\rho_c}{\rho_w} \times \frac{w}{c}\right) \tag{41}$$

where V_c^0 is the initial volume of cement, ρ_c/ρ_w is the cement-to-water mass density ratio, and w/c is the water-to-

cement ratio. Eqs. (33)–(41) form a set of equations that allows determination of the volume fractions for the Level II homogenization (see Table 1):

$$f_{C-S-H} = \frac{V_a + V_b}{V_{II}}; \quad f_X = \frac{V_X}{V_{II}}; \quad f_{CH} = \frac{V_{CH}}{V_{II}};$$
$$f_w = \frac{V_w}{V_{II}}; \quad f_v = \frac{V_v}{V_{II}} \tag{42}$$

and $f_A = 1 - (f_{C-S-H} + \sum_X f_x + f_{CH} + f_w + f_v)$. Note that the initial volume of cement disappears from the determination of the (dimensionless) volume fractions, reducing the number of input parameters to the w/c ratio, the mass fraction of the clinker phases in the cement, and a set of chemical constants summarized in Table 4.

By way of example, Fig. 3 displays, as a function of the overall hydration degree ξ, the evolution of the volume fractions at Level II for a Type I OPC paste: w/c=0.5, m_{C_3S}=0.543, m_{C_2S}=0.187, m_{C_3A}=0.076, m_{C_4AF}=0.073. At complete hydration, the four clinkers are all consumed (f_X=0); f_{C-S-H}=53.8%, f_{CH}=15.6%, and f_A=16.9%. The remaining water, f_w=6.2%, and the formed voids, f_v=7.5%, form the macro-porosity f_w+f_v=13.7%, which is consistent with the results of Hansen [39]. The total porosity is the sum of the intrinsic C–S–H gel porosity and aluminates of approximately 28% and the capillary porosity f_w+f_v=13.7%, i.e., 41.7%, which is close to the value of 39.7±1.1% measured by drying at 105°C, on the same material by Constantinides and Ulm [23].

3.3. Mix-design input parameters

The volume fractions at Levels III and IV are all related to mass proportions of the mix design. The mix proportions are commonly described by the mass of each constituent present in 1 m^3 of mix: the cement content $c=\rho_c f_c^0$ (kg/m^3),

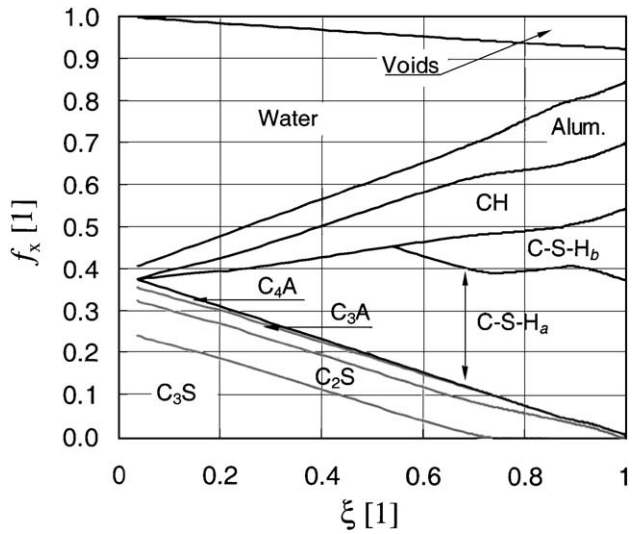

Fig. 3. Evolution of volume fractions of the phases of a w/c=0.5 cement paste (Level II).

Table 5
Set of material-specific model parameters required to calculate the input parameters of the proposed model

Cement	Concrete	
ϕ [cm^2/g]	c [kg/m^3]	$E_{s=g}$ [GPa]
m_{C_3S} [1]	w/c [1]	$\nu_{s=g}$ [1]
m_{C_2S} [1]	s [kg/m^3]	
m_{C_3A} [1]	g [kg/m^3]	
m_{C_4AF} [1]		

the water content $w=\rho_w f_w^0$ (kg/m^3), the sand contents $s=\rho_s f_s^0$ (kg/m^3) (<2 mm, Level III), and the aggregate content $g=\rho_g f_g^0$ (kg/m^3) (>2 mm, Level IV), where ρ_c=3.15 g/cm^3, ρ_w=1.00 g/cm^3, $\rho_s=\rho_g$=2.65 g/cm^3 are the mass densities of cement, water, sand, and aggregate which occupy the volume fractions f_c^0, f_w^0, f_s^0, and f_g^0 in a reference volume. At this scale, the volume fractions of the two-phase hardening material are constant in time and are functions of only the mix-design parameters, i.e., at Level III:

$$f_s = \frac{f_s^0}{f_c^0 + f_w^0 + f_s^0} = \frac{s/\rho_s}{c/\rho_c + w/\rho_w + s/\rho_s}; \quad f_{CP} = 1 - f_s \tag{43}$$

where f_s and f_{CP} are the sand and cement paste volume fractions. Analogously, at Level IV:

$$f_g = \frac{f_s^0}{f_c^0 + f_w^0 + f_s^0 + f_g^0} = \frac{g/\rho_s}{c/\rho_c + w/\rho_w + (s+g)/\rho_s};$$
$$f_M = 1 - f_g \tag{44}$$

where f_g and f_M are the coarse aggregate and mortar volume fractions.

In summary, the application of the proposed micromechanical model to a specific cement-based material requires 11 mix-design specific model parameters, summarized in Table 5, that can be easily obtained from the cement and concrete suppliers. The other model parameters, i.e., the mechanical parameters (Table 2) and the chemical kinetic parameters (Table 3) and chemical volume change parameters (Table 4), are intrinsic values, which are the same for all cement-based materials.

4. Validation and discussion

The predictive capabilities of the model are shown in Fig. 4 in the form of a plot of predicted versus experimental E-modulus values for early-age cement paste, mortar, and concrete found in the open literature [8,12,23,27,40,52]. The individual data sets of the E-modulus evolution versus the hydration degree are shown in Figs. 5–7, comparing results obtained from the micromechanical model with the experimental results. The input parameters for the validation sets are given in Tables 6 and 7. The model accurately

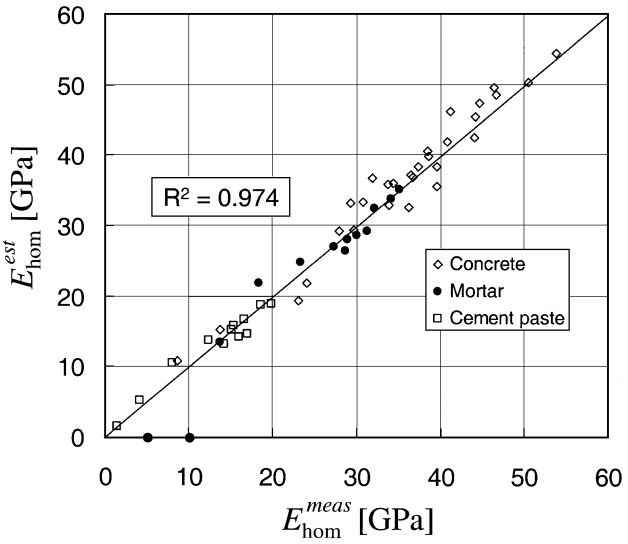

Fig. 4. Predictive capability of the model: predicted versus measured *E*-modulus (data sets [8,12,23,27,40,52]).

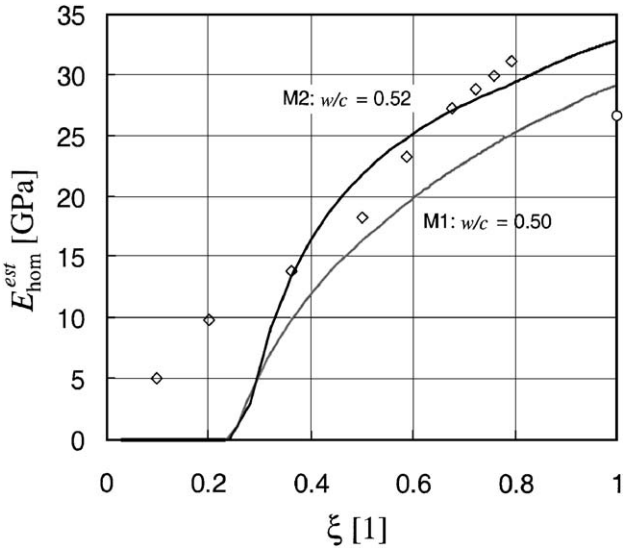

Fig. 6. Comparison of predicted versus measured *E*-modulus of mortar (M1 [23], M2 [40]).

captures the early-age stiffness development of cement-based materials.

There are three model features that deserve particular attention: (i) the percolation threshold, (ii) the role of aggregate inclusions on the macroscopic stiffness evolution, and (iii) the development of the Poisson's ratio at early ages. These aspects are discussed below.

4.1. Percolation threshold

One important model feature is the account of percolation threshold ξ_0 through the use of the SCS scheme at Level II. This percolation threshold corresponds to the percolation of the solid phase, that is, the C–S–H matrix phase, the clinker phases, and the A-phase. More precisely, the percolation threshold of the SCS is associated with a volume fraction of the solid phases (i.e., the phases which exhibit a significant elasticity) greater than 50%, which is equivalent to a porosity smaller than 50%. From Eq. (42), the threshold can be written as:

$$\xi \geq \xi_0 \Longleftrightarrow f_{C-S-H} + \sum_X f_X + f_{CH} + f_A \geq 0.5;$$

$$f_w + f_v \leq 0.5 \tag{45}$$

Unfortunately, there are few experimental values of the percolation threshold reported in the open literature:

- De Schutter and Taerwe [12] determined the percolation threshold by extrapolating stiffness values measured at

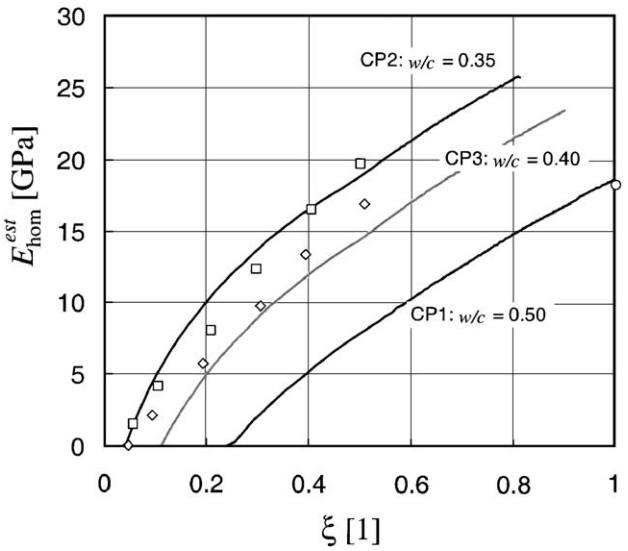

Fig. 5. Comparison of predicted versus measured *E*-modulus of cement paste (CP1 [23], CP2+CP3 [40]).

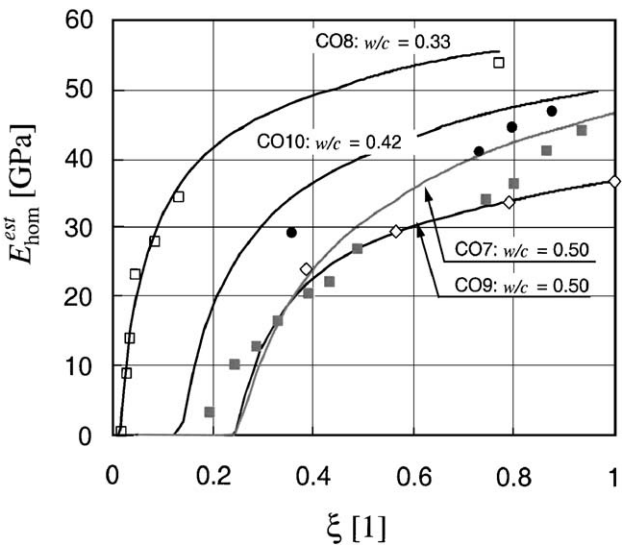

Fig. 7. Comparison of predicted versus measured *E*-modulus of concrete (CO7+CO8 [8], CO9 [12], CO10 [27]).

Table 6
Input parameters of validation set at levels I and II

References	Type	ϕ [cm^2/g]	m_{C_3S} [1]	m_{C_2S} [1]	m_{C_3A} [1]	m_{C_4AF} [1]	w/c [1]
Constantinides and Ulm [23]	CP1+M1	3602	0.543	0.187	0.076	0.073	0.50
Boumiz et al. [40]	CP2	7600	0.663	0.121	0.106	0.009	0.35
	CP3	7600	0.663	0.121	0.106	0.009	0.40
	M2	7600	0.638	0.089	0.082	0.062	0.52
	M3	7600	0.620	0.113	0.083	0.060	0.39
Granger [52]							
Chooz	CP4+CO1	3600	0.645	0.130	0.060	0.115	0.54
Penly	CP5+CO2	3600	0.560	0.180	0.052	0.110	0.58
Flamanville	CP6+CO3	3600	0.560	0.180	0.052	0.110	0.48
Paluel	CP7+CO4	3600	0.560	0.180	0.052	0.110	0.48
CivauxB11	CP8+CO5	3600	0.686	0.050	0.068	0.087	0.56
CivauxBHP	CP9+CO6	3600	0.686	0.050	0.068	0.087	0.61
Laplante [8]							
BO	CO7	3466	0.607	0.187	0.028	0.122	0.50
BTHP	CO8	3466	0.607	0.187	0.028	0.122	0.33
De Schutter and Taerwe [12]	CO9	5320	0.594	0.118	0.078	0.100	0.50
Le Roy [27]							
BO5	CO10	3466	0.607	0.187	0.028	0.122	0.42

higher hydration degrees to zero-stiffness values. For a concrete prepared at w/c=0.5, they reported percolation threshold that varied between ξ_0=0.17 and ξ_0=0.25. These values are on the same order as the percolation threshold predicted by the micromechanical model (see CO9 in Fig. 7).

- Boumiz et al. [40] determined percolation thresholds by combining ultrasonic measurements with hydration heat measurements on cement pastes (CP2 w/c=0.35 and CP3 w/c=0.40, see Fig. 5) and mortars (M2 w/c=0.52, see Fig. 6). The time of percolation was set equal to the material age at which the first significant shear ultrasonic velocity was measured. Parallel hydration heat measurements allowed replacing the time by the hydration degree threshold ξ_0. The values determined by this method differ from the ones predicted by the micromechanical model, for both cement paste ($\xi_{0,CP2}^{mod}$=0.046 versus $\xi_{0,CP2}^{exp}$=0.015; $\xi_{0,CP3}^{mod}$=0.11 versus ξ_0^{exp}=0.021) and mortar ($\xi_{0,M2}^{mod}$=0.246 versus $\xi_{0,M2}^{exp}$=0.015). The difference may well result from the relatively low solid volume fraction threshold (Eq. (45)) of the SC upscaling scheme, which could lead to an overestimation of the hydration degree percolation threshold ξ_0. On the other hand, the difference may well be related to the experimental difficulty to accurately determine the hydration degree by calorimetric measurements in the very first hours of hydration, given that heat of hydration is only produced beyond the initial degree of hydration $\xi_{X,0}$ of each clinker phase (see Table 3). In other words, the experimental error may well be on the order of $\Delta\xi$=0.03–0.06, that is on the order of the difference between experimental and predicted percolation threshold.

Finally, it is interesting to note that the percolation threshold defined by Eq. (45) translates into a critical w/c

Table 7
Input parameters of validation set at levels III and IV

References	Type	c [kg/m^3]	s [kg/m^3]	g [kg/m^3]	$E_{s=g}$ [GPa]	$\nu_{s=g}$ [1]
Constantinides and Ulm [23]	CP1+M1	620	1241	–	50	0.30
Boumiz et al. [40]	M2	569	1390	–	45	0.30
	M3	730	1297	–	45	0.30
Granger [52]						
Chooz	CP4+CO1	350	836	1130	70	0.27
Penly	CP5+CO2	350	752	1012	65	0.27
Flamanville	CP6+CO3	375	795	1040	55	0.22
Paluel	CP7+CO4	375	772	1048	65	0.27
CivauxB11	CP8+CO5	350	772	1100	61	0.28
CivauxBHP	CP9+CO6	266	879	1133	61	0.28
Laplante [8]						
BO	CO7	342	670	1200	65	0.23
BTHP	CO8	398	709	1216	65	0.23
De Schutter and Taerwe [12]	CO9	300	670	1280	45	0.23
Le Roy [27]						
BO5	CO10	355	696	1204	75	0.23

ratio, below which the model predicts a zero percolation threshold, i.e., $\xi_0=0$, for which $f_v(\xi=0)=0$, and thus, $f_w(\xi=0)=f_w^0\leq 0.5$. Indeed, from Eqs. (34) and (41):

$$\xi_0=0 \Longleftrightarrow f_w^0=\frac{V_w^0}{V_{II}}=\frac{\frac{\rho_c}{\rho_w}\times\frac{w}{c}}{1+\frac{\rho_c}{\rho_w}\times\frac{w}{c}}\leq 0.5 \Rightarrow \frac{w}{c}\leq\frac{\rho_w}{\rho_c}=0.318 \quad (46)$$

For $w/c>\overline{w/c}=0.318$, the percolation threshold ξ_0 increases quasilinearly with the w/c ratio, as displayed in Fig. 8 (determined with the input parameter of CP1). While the value of the critical w/c ratio of $\overline{w/c}=0.318$ is related to the relatively low solid volume fraction percolation threshold of the SCS, the dependence of ξ_0 on w/c is consistent with percolation theory applied to cement-based materials [42] and experimental observations [12]. On the other hand, for w/c ratios smaller than $\overline{w/c}$, the model considers that the unhydrated cement grains are initially in contact so that the solid phase percolates. This situation, however, never occurs in cement-based materials, in which superplasticizer prevents the grain-to-grain (dry) contact by coating the clinker surfaces. From a mechanical point of view, this coating deactivates the force transmission from clinker to clinker grain, thus neutralizing the mechanical contribution of the clinker elasticity to the overall elasticity. This coating effect, which is not related to the hydration reactions but to another chemophysical phenomenon, is not considered in our micromechanical model, and its consideration would require consideration of the coating activity of superplasticizer. This can be achieved, in a first approach, by means of an activation degree $\eta\in[0,1]$ that describes the mechanical activity of the clinker elasticity, that is:

$$k_X^{eff}=\eta\times k_X;\quad \mu_X^{eff}=\eta\times\mu_X \quad (47)$$

Initially $\eta=0$, and $\eta\rightarrow 1$ with the loss of the superplasticizer. The effect of this activation factor for a low w/c =0.33 concrete is shown in Fig. 7 (CO8). The hydration degree was determined with the proposed model, and $\eta=H(t-\tau_r)$ was assumed in the micromechanical model, where $H(x)$ is the Heaviside function, and τ_r=10 h, the retardation time of the setting process due to the use of superplasticizer. This adds a further input parameter to the model, but one that is independent of the hydration reactions.

Finally, the percolation threshold ξ_0 appears to have a strong influence on the asymptotic E-modulus reached when the hydration is completed or stopped due to a lack of water. With all other parameters constant, the model predicts that the smaller the percolation threshold, the higher the final E-modulus. For example, the final E-modulus of concrete CO8 (ξ_0=0, w/c=0.33) in Fig. 7 is higher than the E-modulus of concrete CO10 (ξ_0=0.12, w/c=0.42), despite the lower stiffness of the inclusions of concrete CO8 (see Table 7), and the smaller final value of the hydration degree of CO8 ($\xi_{\infty,\,CO8}$=0.77 versus, $\xi_{\infty,\,CO10}$=0.97). Hence, it may be suggested from the micromechanical model that the well-known higher stiffness of low w/c ratio cement-based materials results from their lower percolation threshold ξ_0.

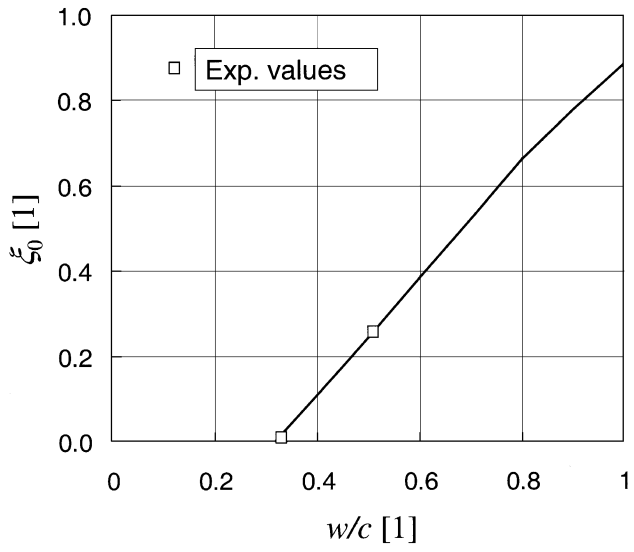

Fig. 8. Influence of w/c ratio on the percolation threshold ξ_0 (determined with input parameters of CP1; Experimental values from Refs. [12,40]).

4.2. Role of inclusions

The model reveals an interesting feature of aging elasticity related to the presence of sand and aggregate in the composite at Levels III and IV, respectively. The E-modulus of cement paste, which represents the matrix at Level III, develops almost linearly with the hydration degree (see Fig. 5). By contrast, the addition of sand inclusions in mortar, and aggregates in concrete, leads to a deviation from this linear behavior of the paste: the modulus increases much stronger at early hydration degrees (“elastic stiffening”) but then levels off (see Figs. 6 and 7). The higher the inclusion volume fraction, the stronger this elastic stiffening following the percolation threshold ξ_0. This stronger early-age stiffening also affects the final value. For instance, despite a 10% lower E-modulus of sand in mortar M2 over M1, the greater inclusion volume fraction of $f_{s,M2}$=0.53 compared to $f_{s,M1}$=0.48 leads to a 10% greater final E-modulus of M2 over M1 (see Fig. 6). Analogously, for concrete (see Fig. 7), the greater inclusion volume fraction of concrete CO9 of $f_{s,CO9}+f_{g,CO9}$=0.75 compared to $f_{s,CO7}+f_{g,CO7}$=0.71 of CO7 compensates the lower inclusion stiffness of E_s=45 GPa of concrete CO9 compared to E_s=65 GPa of CO7. These two effects, inclusion stiffness versus inclusion volume fraction, are in

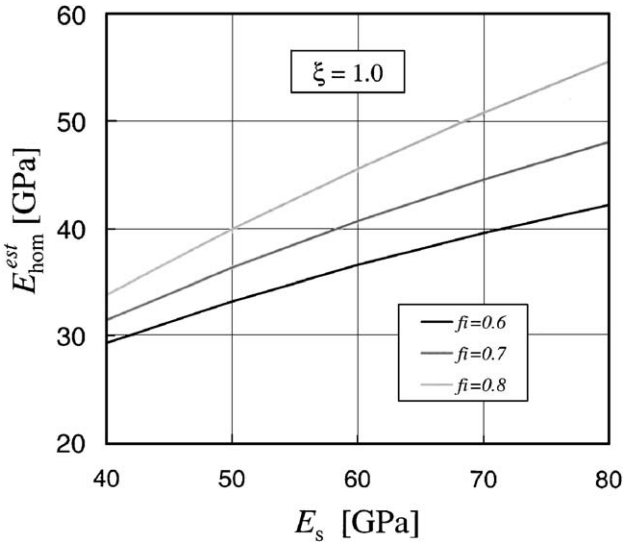

Fig. 9. Influence of inclusion stiffness E_s and inclusion volume fraction $f_i=f_s+f_g$ on the E-modulus of concrete (calculated for $\xi=1.0$).

competition during the hydration process: for $\xi \leq 0.4$, the inclusion fraction $f_i=f_s+f_g$ seems to have a stronger influence than the E-modulus E_s on the evolution of the composite E-modulus of cement-based materials, and for higher hydration degrees, it is the inverse. Fig. 9 displays the composite E-modulus as a function of the inclusion stiffness for different inclusion fractions. For a given set of mix parameters (here mix proportions of concrete CO9), a simple rule can be established: a decrease of 10% of the volume fraction of inclusions is roughly compensated by an increase of 10 GPa of the inclusion stiffness E_s.

Finally, we note that the micromechanical model employed at Levels III and IV slightly overestimates the stiffness value of the composite material, mortar, and concrete. This overestimation is due to the effect of the ITZ, which was not taken into account in the two-phase model. A three-phase model that considers the ITZ would be required to improve the accuracy of the proposed micromechanical model.

4.3. Poisson's ratio

The evolution of the Poisson's ration ν^{est}_{hom} during the hydration of cement-based materials is related to the evolution of the effective shear modulus to bulk modulus ratio $\mu^{est}_{hom}/k^{est}_{hom}$:

$$\nu^{est}_{hom} = \frac{3 - 2\mu^{est}_{hom}/k^{est}_{hom}}{6 + 2\mu^{est}_{hom}/k^{est}_{hom}} \quad (48)$$

Given the negligible shear-to-bulk modulus ratio $\mu^{est}_{hom}/k^{est}_{hom} \rightarrow 0$ of water-dominated suspensions, it is generally accepted that the Poisson's ratio of the fresh mix should be close to the Poisson's ratio of water $\nu=0.5$ [12]. During the early stages of hydration, the experimental values of Boumiz et al. [40] and Byfors [5] provide evidence of a decrease of the Poisson's ratio from $\nu^{est}_{hom}=0.48$ to roughly $\nu^{est}_{hom}=0.15$. After the percolation threshold, Byfors [5] and De Schutter and Taerwe [12] reported an increase of the Poisson's ratio to a final value close to $\nu=0.25$; this increase has been attributed to the progressive hardening of the material. These experimental observations highlight the complex role played by the different components of cement-based materials on the shear-to-bulk modulus ratio, which increases below the percolation threshold from $\mu^{est}_{hom}/k^{est}_{hom}=0.04$ to $\mu^{est}_{hom}/k^{est}_{hom}=0.91$ and decreases beyond ξ_0 to $\mu^{est}_{hom}/k^{est}_{hom}=0.60$.

To evaluate the role of water in the development of the Poisson's ratio, two simulations were performed with the micromechanical model; one in which the compressibility of the water phase was considered (i.e., $k_w=2.18$ GPa; $\mu_w=0$), the other in which the compressibility was neglected (i.e., $k_w=\mu_w=0$.). The predicted development of the homogenized Poisson's ratio ν^{est}_{hom} for the two limit cases is displayed in Fig. 10. The simulations were carried out for the mix proportions of cement paste CP1 and mortar M1. We note:

- When the compressibility of water is taken into account, the effective Poisson's ratio ν^{est}_{hom} is a continuously decreasing function of the hydration degree, and the rate of decrease is amplified by the presence of inclusions (mortar M1). Below the percolation threshold ($\xi_0=0.25$), the model predicts for the cement paste a decrease from $\nu^{est}_{hom}=0.50$ to $\nu^{est}_{hom}=0.37$. This confirms qualitatively that the experimentally observed decrease of the Poisson's ratio is due to the consumption of water in the early stages of the hydration reaction. This decrease is higher at lower w/c ratios.
- When the compressibility of the water is neglected, ν^{est}_{hom} is a continuously increasing function of the hydration

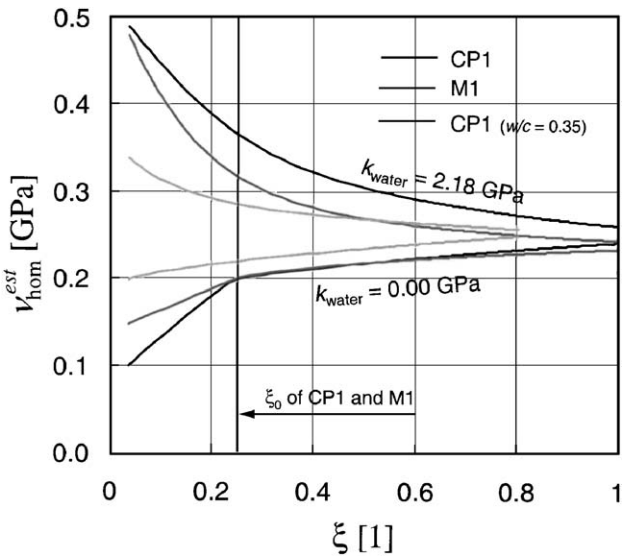

Fig. 10. Evolution of Poisson's ratio of cement paste CP1 and mortar M1 and influence of a reduced w/c ratio (CP1 with $w/c=0.35$).

degree. Beyond the percolation threshold, the model predicts an increase from ν_{hom}^{est}=0.20 to ν_{hom}^{est}=0.25, which is little affected by the presence of inclusions. This confirms that any increase of the Poisson's ratio is associated with the solid stiffness evolution.

- As ξ approaches 1, both models converge towards an asymptotic value that is not affected by the compressibility of the remaining water in the mix, nor by the sand inclusions. The value of ν_{hom}^{est} calculated for cement paste CP1 is in good agreement with the experimental value ν_{hom}^{exp} =0.24 reported by Le Bellego [58] for similar cement-based materials.

The two limiting cases studied here highlight the effect of the percolated phase on the effective shear-to-bulk modulus ratio and on the Poisson's ratio. Below the percolation threshold, the water phase is continuous, and its bulk modulus, therefore, strongly affects the composite Poisson's ratio. Beyond the percolation threshold, the solid phase is continuous and dominates the increase of the Poisson's ratio of the composite. The 'real' evolution of the Poisson's ratio lies within these limiting cases. Since our micromechanics model is based on only one solid percolation threshold, i.e., Eq. (45), it cannot capture the continuous transition from the water-dominated effective composite material behavior of the fluid suspension to the solid-dominated effective composite material behavior of the hardening solid phase. Such a model requires consideration of a water percolation threshold in addition to the solid percolation threshold. It is suggested that once the water phase becomes discontinuous, the water bulk modulus k_w ceases to affect the overall elasticity of the composite, marking the switch from a decreasing Poisson's ratio to an increasing Poisson's ratio.

5. Conclusions

Continuum micromechanics combined with advanced cement chemistry hydration models provides a rational tool to study the aging elasticity of cement-based materials, with a minimum of intrinsic material properties (same for all cement-based materials), and 11 mix-design specific model parameters that can be easily obtained from the cement and concrete supplier. The key to the model is the four microstructure levels of cement-based composite materials, which allow the gap between the physical chemistry of cement hydration and the mechanics of cement-based materials to be bridged. We suggest:

1. The solid percolation threshold derived from micromechanics theory is a function of the *w*/*c* ratio. For the employed SCS, a critical *w*/*c* ratio of $\overline{w/c} = 0.318$ defines a zero percolation threshold. Below this value, the solid phase percolates at the onset of hydration, once the activity of superplasticizer ceases to coat the clinker phases. Beyond this value, the percolation threshold increases quasilinearly with increasing *w*/*c* ratio. This percolation threshold affects significantly the final stiffness value of the hardened cement-based material.
2. The two effects of sand and aggregate inclusions on the composite stiffness evolution relate to the inclusion volume fractions and inclusion stiffness. At early stages of hydration (around the percolation threshold), the first effect dominates over the latter, and for higher hydration degrees, it is the inverse. For a given set of mix parameters, a decrease of 10% of the volume fraction of inclusions can be compensated by an increase of 10 GPa of the inclusions *E*-modulus. This simple rule can be employed for a fine-tuned mix design of fast-stiffening or slow-stiffening early-age concrete that have the same final service state *E*-modulus.
3. The development of the Poisson's ratio at early ages relates to (at least) two percolation thresholds: one for the water phase and one for the solid phase. As long as the water phase is continuous, the Poisson's ratio decreases due to the consumption of water in the hydration reactions. When the water phase becomes discontinuous, the development of the Poisson's ratio becomes dominated by the solid stiffening, leading to an increase of the Poisson's ratio.

Finally, a refinement of the model components on both the micromechanics side and the cement chemistry side can still improve the accuracy of the prediction of the model. For instance, on the micromechanics side, consideration of the ITZ at Levels III and IV will surely improve the predictive capabilities of the model, particularly for high *w*/*c* ratio mortars and concretes. On the cement chemistry side, an improved understanding of the effects of superplasticizers on the early stages of hydration will extend the domain of application of the model to very low *w*/*c* ratio cement-based materials.

Acknowledgements

The authors gratefully acknowledge the financial support of this study by the Swiss National Science Foundation (SNF), mediated through the research committee of the Swiss Federal Institute of Technology in Lausanne, Switzerland, enabling the postdoctoral work of the first author at MIT. The authors also acknowledge the valuable review comments of the original manuscript. The detailed description of the Elements of continuum micromechanics in the revised version was suggested by one of the reviewers.

Appendix A. Kinetic laws

This appendix shows the deviation of the normalized affinity expression (22) for the nucleation and growth

kinetics based on Avrami's model. The Avrami equation reads [54]:

$$-\ln[1-(\alpha-\alpha_0)] = [k(t-t_0)]^{\kappa} \tag{49}$$

where α is the degree of reaction at time t, k is the rate constant, and κ is an exponent. The constants α_0 and t_0 define the degree of reaction and time at which the nucleation and growth kinetic regime begins. Differentiating Eq. (49) with respect to time, a rate expression as a function of time is obtained (see Ref. [55]):

$$\frac{d\alpha}{dt} = mk^{\kappa}(t-t_0)^{\kappa-1}\exp[-k^{\kappa}(t-t_0)^{\kappa}] \tag{50}$$

Replacing the time $t-t_0$ by $\alpha-\alpha_0$ according to Eq. (49), the rate expression as a function of the reaction degree reads:

$$\frac{d\alpha}{dt} = \kappa k(1-(\alpha-\alpha_0))(-\ln(1-(\alpha-\alpha_0)))^{1-\frac{1}{\kappa}} \tag{51}$$

Expressed in the dimensionless form (Eq. (20)), we obtain:

$$\tau\frac{d\alpha}{dt} = \tilde{A}^{A}(\alpha) \tag{52}$$

where the normalized affinity $\tilde{A}^{A}(\alpha)$ and the characteristic time τ read:

$$\tilde{A}^{A}(\alpha) = \frac{1-(\alpha-\alpha_0)}{(-\ln(1-(\alpha-\alpha_0)))^{\frac{1}{\kappa}-1}}; \quad \tau = \frac{1}{\kappa k} \tag{53}$$

These are Eqs. (22) and (23), for which the constants are given in Table 3 determined from given values for κ and k found in the literature [31].

Finally, expression (24) of the normalized affinity for the diffusion-controlled hydration kinetics is derived in an analogous way, using the integrated form of the solution of Fuji and Kondo [56].

References

[1] R. Springenschidt (Ed.), Thermal Cracking in Concrete at Early Age, Proceedings no. 25 of the International RILEM Symposium, Munich, E&FN Spon, London, UK, 1994.

[2] P. Acker, F.-J. Ulm, Creep and shrinkage of concrete: physical origins, practical measurements, Nuclear Engineering and Design 203 (2–3) (2001) 143–158.

[3] A. Bentur (Ed.), Early Age Cracking in Cementitious Systems, State of the Art Report of the RILEM Technical Committee TC 181-EAS, Haifa, RILEM, France, 2002.

[4] A.G.A. Saul, Principles underlying the steam curing of concrete at atmospheric pressure, Magazine of Concrete Research 2 (6) (1951) 127–140.

[5] J. Byfors, Plain concrete at early age, PhD. thesis report FO 3:80, Swedish Cement and Concrete Research Institute, Stockholm, 1980.

[6] M. Regourd, E. Gauthier, Behavior of cement under accelerated hardening, Annales de l'Institut Technique du Batiment et des Travaux Publics 387 (1980) 65–96.

[7] M. Emborg, Thermal stresses in concrete structures at early ages. PhD. dissertation, Lulea University of Technology, Lulea, 1989.

[8] P. Laplante, Mechanical properties of hardening concrete: a comparative analysis of ordinary and high performance concretes, Research report LPC OA13, Laboratoire Central des Ponts et Chaussés, Paris, 1993, in French.

[9] M. Laube, Constitutive model for the analysis of temperature-stresses in massive structures, PhD. dissertation, TU Braunschweig, Braunschweig, 1990, in German.

[10] K. Van Breugel, Simulation of hydration and formation of structure in hardening cement-based materials, PhD. dissertation, TU Delft, Delft, 1991.

[11] F.-J. Ulm, O. Coussy, Modeling of thermo-chemo-mechanical couplings of concrete at early ages, Journal of Engineering Mechanics, ASCE 121 (7) (1995) 785–794.

[12] G. De Schutter, L. Tearwe, Degree of hydration-based description of mechanical properties of early age concrete, Materials and Structures 29 (7) (1996) 335–344.

[13] Z.P. Bažant, S. Prasannan, Solidification theory for concrete creep: I. Formulation, Journal of Engineering Mechanics, ASCE 115 (8) (1989) 1691–1703.

[14] F.-J. Ulm, O. Coussy, Strength growth as chemo-plastic hardening in early age concrete, Journal of Engineering Mechanics, ASCE 122 (12) (1996) 1123–1132.

[15] F.-J. Ulm, O. Coussy, Couplings in early-age concrete: from material modeling to structural design, International Journal of Solids and Structures 35 (31–32) (1998) 4295–4311.

[16] F.-J. Ulm, O. Coussy, What is a massive concrete structure at early ages? Some dimensional arguments, Journal of Engineering Mechanics, ASCE 127 (5) (2001) 512–522.

[17] J. Sercombe, C. Hellmich, F.J. Ulm, H. Mang, Modeling of early age creep of shotcrete: I. model and model parameters, Journal of Engineering Mechanics, ASCE 126 (3) (2000) 284–291.

[18] C. Hellmich, J. Sercombe, F.-J. Ulm, H. Mang, Modeling of early age creep of shotcrete: I. application to tunneling, Journal of Engineering Mechanics, ASCE 126 (3) (2000) 292–299.

[19] C. Hellmich, H. Mang, F.-J. Ulm, Hybrid method for quantification of stress states in shotcrete tunnel shells: combination of 3D in situ displacement measurements and thermoplastic material law, Computers and Structures 79 (2000) 2103–2115.

[20] M. Cervera, J. Oliver, T. Prato, Thermo-chemo-mechanical model for concrete: I. Hydration and aging, Journal of Engineering Mechanics, ASCE 125 (9) (1999) 1018–1027.

[21] M. Cervera, J. Oliver, T. Prato, Thermo-chemo-mechanical model for concrete: II. Damage and creep, Journal of Engineering Mechanics, ASCE 125 (9) (1999) 1028–1039.

[22] P. Acker, Micromechanical analysis of creep and shrinkage mechanisms, in: F.-J. Ulm, Z.P. Bažant, F.H. Wittmann (Eds.), Creep, Shrinkage and Durability Mechanics of Concrete and Other Quasi-Brittle Materials, Proc. of the Sixth International Conference CONCREEP6, Elsevier, Oxford, UK, 2001, pp. 15–25.

[23] G. Constantinides, F.-J. Ulm, The effect of two types of C–S–H on the elasticity of cement-based materials: results from nanoindentation and micromechanical modeling, Cement and Concrete Research (submitted for publication).

[24] T.J. Hirsch, Modulus of elasticity of concrete affected by elastic moduli of cement paste matrix and aggregate, Journal of the American Concrete Institute 59 (3) (1962) 427–452.

[25] U.J. Counto, The effect of the elastic modulus of the aggregate on the elastic modulus, creep and creep recovery of concrete, Magazine of Concrete Research 16 (48) (1964) 129–138.

[26] A. Guidoum, 3D numerical simulation of the behavior of concretes as granular composites, PhD. dissertation No. 1310, Swiss Federal Institute of Technology in Lausanne, Lausanne, 1995, in French.

[27] R. Le Roy, Instantaneous and time-dependent deformations of high performance concretes, Research report LPC OA22, Laboratoire Central des Ponts et Chaussées, Paris, 1996, in French.

[28] A. Zaoui, Continuum micromechanics—a survey, Journal of Engineering Mechanics, ASCE 128 (8) (2002) 808–816.

[29] J.J. Thomas, S.A. FitzGerald, D.A. Neumann, R.A. Livingston, State of water in hydrating tricalcium silicate and portland cement pastes as

measured by Quasi-Elastic Neutron Scattering, Journal of the American Ceramic Society 84 (8) (2001) 1811–1816.
[30] P.D. Tennis, H.M. Jennings, A model for two types of calcium silicate hydrate in the microstructure of portland cement paste, Cement and Concrete Research 30 (6) (2000) 855–863.
[31] R. Berliner, M. Popovici, K.W. Herwig, M. Berliner, H.M. Jennings, J.J. Thomas, Quasielastic neutrons scattering study of the effect of water-to-cement ratio on the hydration kinetics of tricalcium silicate, Cement and Concrete Research 26 (2) (1998) 231–243.
[32] J.H. Taplin, A method for following the hydration reaction in portland cement paste, Australian Journal of Applied Science 10 (1959) 329–345.
[33] I.G. Richardson, The nature of C–S–H in hardened cement, Cement and Concrete Research 29 (1999) 1131–1147.
[34] G.W. Groves, TEM studies of cement hydration, Materials Research Society Symposium Proceedings 85 (1987) 3–12.
[35] H.F.W. Taylor, Cement Chemistry, Academic Press, New York, 1990.
[36] K.L. Scrivener, H.H. Patell, P.L. Pratt, L.J. Parrott, Analysis of phases in cement paste using backscattered electron images, methanol adsorption and thermogravicmetric analysis, Materials Research Society Symposium Proceedings 85 (1985) 67–76.
[37] S. Diamond, D. Bonen, Microstructure of hardened cement paste—a new interpretation, Journal of the American Ceramic Society 76 (12) (1993) 2993–2999.
[38] H.M. Jennings, A model for the microstructure of calcium silicate hydrate in cement paste, Cement and Concrete Research 30 (1) (2000) 101–116.
[39] T.C. Hansen, Physical structure of hardened cement paste. A classical approach, Materials and Structures 19 (114) (1986) 423–436.
[40] A. Boumiz, C. Vernet, F.C. Tenoudji, Mechanical properties of cement pastes and mortars at early ages. Evolution with time and degree of hydration, Advanced Cement-Based Materials 3 (1992) 94–106.
[41] P. Acker, Mechanical behavior of concrete: a physico-chemical approach, Research report LPC 152, Laboratoire Central des Ponts et Chaussées, Paris, 1988, in French.
[42] E.J. Garboczi, Computational materials science of cement-based materials, Materials and Structures 26 (2) (1993) 191–195.
[43] G.Q. Li, Y. Zhao, S.S. Pang, Y.Q. Li, Effective Young's modulus estimation of concrete, Cement and Concrete Research 29 (9) (1999) 1455–1462.
[44] J.D. Eshelby, The determination of the elastic field in an ellipsoidal inclusion, Proceedings of the Royal Society of London A 241 (1957) 376–392.
[45] T. Mori, K. Tanaka, Average stress in matrix and average elastic energy of materials with misfitting inclusions, Acta Metallurgica 21 (5) (1973) 1605–1609.
[46] A.V. Hershey, The elasticity of an isotropic aggregate of anisotropic cubic crystals, Journal of Applied Mechanics 21 (1954) 236.
[47] E. Kröner, Bounds for effective elastic moduli of disordered materials, Journal of Mechanics and Physics of Solids 24 (1977) 137–155.
[48] J.J. Beaudoin, Comparison of mechanical properties of compacted calcium hydroxide and Portland cement paste systems, Cement and Concrete Research 13 (1983) 319–324.
[49] F.H. Wittmann, Estimation of the modulus of elasticity of calcium hydroxide, Cement and Concrete Research 16 (6) (1986) 971–972.
[50] P.J.M. Monteiro, C.T. Chang, The elastic moduli of calcium hydroxide, Cement and Concrete Research 25 (8) (1995) 1605–1609.
[51] K. Velez, S. Maximilien, D. Damidot, G. Fantozzi, F. Sorrentino, Determination by nanoindentation of elastic modulus and hardness of pure constituents of Portland cement clinker, Cement and Concrete Research 31 (4) (2001) 555–561.
[52] L. Granger, Time-dependent behavior of concrete in nuclear tanks: analysis and modeling, Research report LPC OA21, Laboratoire Central des Ponts et Chaussées, Paris, 1996, 1995, in French.
[53] P.W. Atkins, Physical Chemistry, 5th ed., Oxford Univ. Press, Oxford, 1994.
[54] M. Avrami, Journal of Chemical Physics 7 (1939) 1103–1108.
[55] J.J. Thomas, H.M. Jennings, Effect of D_20 and mixing on the early hydration kinetics of tricalcium silicate, Chemistry of Materials 11 (1999) 1907–1914.
[56] K. Fuji, W. Kondo, Journal of American Ceramics Society 57 (1974) 492–502.
[57] T.C. Powers, T.L. Brownyard, Studies of the physical properties of hardened Portland cement paste, Journal of the American Concrete Institute 18 (1946) 101–132.
[58] C. Le Bellego, Chemo-mechanical couplings in concrete structures submitted to leaching: experimental study and numerical analysis, PhD. thesis report, LMT-Cachan, Cachan, 2001, in French.